

Effectiveness of the Self-Consistent Harmonic Approximation in ferromagnets with dipolar interactions

A. R. Moura^{1,*}

¹*Departamento de Física, Universidade Federal de Viçosa, 36570-900, Viçosa, Minas Gerais, Brazil*
(Dated: June 7, 2022)

Among the various methods for treating magnetic models, the Self-Consistent Harmonic Approximation (SCHA) has successfully described ferro and antiferromagnetism in many different scenarios. In particular, the SCHA is a valuable and easy formalism for determining transition temperatures as, for example, the Berezinskii-Kosterlitz-Thouless. The heart of the method includes thermal fluctuations through of a renormalization parameter depending on temperature. Nevertheless, most of the work has been done considering only short-range interactions, which results in an incomplete description of actual magnetic samples. Here, we generalize the SCHA to include the dipolar interaction in the thermodynamic analysis. The method is applied to analyze the well-known Europium Chalcogenides EuO and EuS. The SCHA results are in good agreement with the experimental measurements.

Keywords: Dipolar interaction; Self-Consistent Harmonic Approximation; magnetism; Europium Chalcogenides

I. INTRODUCTION AND MOTIVATION

The description of magnetism in condensed matter physics involves a diversified set of theoretical tools. For a long time, the bosonic representations, for example, have been widely used to investigate all kinds of magnetic properties, spin excitations, and phase transitions in ferro (FM) and antiferromagnetic (AFM) models. The main concept is the replacement of the spin operators by annihilation/creation bosonic ones. Since there are many bosonic representations, one should choose the more appropriate formalism according to the model's dimensionality, temperature, spin interactions, and/or symmetries. At low temperatures (below the ordering temperature), it is usual to adopt the Holstein-Primakoff representation [1] since the spontaneous symmetry breaking justifies the series expansion of the spin operators in lower orders of the magnon occupation $n = a^\dagger a \ll 1$ [2]. In the lowest order, we have the traditional linear spin-wave theory, which is a reasonable picture of magnons weakly coupled. On the other hand, phases with intact symmetry are better described by using the Schwinger bosonic representation [2–5], although three-dimensional models require special attention close to the transition temperature [6]. In general, the mean-field approach of the Schwinger formalism is sufficient for most of the scenarios; however, in frustrated models, the inclusion of Gaussian fluctuations should be considered [7–10], providing some extra complexity to the model. Moreover, it is also possible to represent the spin field by the non-linear sigma model O(3) [2, 11, 12] and then quantize the field fluctuations by standard techniques of quantum field theory (furthermore, note that in the AFM case, one should be careful with the topological phase). In addition, the Self-Consistent Gaussian Ap-

proximation (SCGA) [13] presents a purpose similar to the Self-Consistent Harmonic Approximation (SCHA). In the SCGA, the thermodynamics of a classical spin model is evaluated through self-consistent equations depending on the magnetization and their quadratic fluctuations. In this case, the Gaussian corrections are introduced by considering spin cumulants [14, 15] in the statistical averages. The SCGA formalism provides good results; however, the number of self-consistent parameters is larger than the SCHA, and the quantization is more challenging to implement.

The Self-Consistent Harmonic Approximation is another practical approach for solving spin models [16]. Classically, the spin fields can be written using the phase angle φ around the z-axis and the spin component S^z . It is clear that φ and S^z composite a pair of canonically conjugate fields that obey the Poisson bracket $\{\varphi_i, S_j^z\} = \delta_{ij}$. In the quantum point of view, the development is similar with the fields being replaced by operators that satisfy the commutation relation $[\varphi_i, S_j^z] = i\hbar\delta_{ij}$. Over the years, Pires *et al.* have applied the SCHA method to evaluate the critical temperature [17–22], the topological BKT transition [17, 20, 23–33], and the large-D quantum phase transition [34–38] in a wide variety of magnetic models. Similar to the linear spin-wave theory, in the SCHA, we expand the Hamiltonian up to second order in φ and S^z . However, higher-order contributions are taken into account through a renormalization parameter ρ that depends on temperature. The renormalization temperature is determined by a self-consistent equation that normally presents a fast convergence. Therefore, the SCHA method provides an easy and efficient alternative for investigating spin models, mainly in determining thermal and quantum phase transitions without the disadvantages of the usual bosonic formalisms. In addition, Moura and Lopes have demonstrated that, since φ and S^z are canonically conjugated, SCHA is the natural choice to describe coherent states in magnetic models

* antoniormoura@ufv.br

[39], making SCHA very useful for describing the magnetization precession in spintronics.

Despite the success of the SCHA to describe spin models with short-range interactions, there are only a couple of works considering Hamiltonians with long-range interactions. Pires investigated the phase transition of the Heisenberg model with ferromagnetic long-range interaction decaying as r^{-p} [18], and Moura generalized the results to the anisotropic Heisenberg model [40]. In both cases, the long-range interaction was considered isotropic, limiting the possible applications. This paper, will present a complete development of the SCHA that includes the dipolar interaction. As it is well-known, the dipolar interaction is an anisotropic long-range interaction that decays as r^{-3} . In general, the dipolar interaction is weak, compared to the exchange coupling, and insufficient to sustain an ordered phase by itself. However, the dipolar field has a fundamental role in the description of ferromagnetic insulators, as the ferromagnetic Yttrium-Iron-Garnet, which is commonly used in spintronics [41]. Furthermore, to verify the obtained results, the SCHA is used to determine the thermodynamics of the ferromagnetic Europium Chalcogenides EuS and EuO [42]. In both cases, the results agree with the literature.

II. THE SCHA METHOD

We will consider a ferromagnetic insulator in a cubic crystalline lattice with an exchange interaction between nearest neighbors. In the SI unit system, the Heisenberg Hamiltonian endowed with dipolar interaction is given by

$$H = -J \sum_{\langle ij \rangle} \mathbf{S}_i \cdot \mathbf{S}_j + \frac{\mu_0 (g\mu_B)^2}{4\pi} \sum_{ij} \left[\frac{\mathbf{S}_i \cdot \mathbf{S}_j}{r_{ij}^3} - 3 \frac{(\mathbf{S}_i \cdot \mathbf{r}_{ij})(\mathbf{S}_j \cdot \mathbf{r}_{ij})}{r_{ij}^5} \right], \quad (1)$$

where the first sum is done over nearest neighbors and the second one is evaluated over each spin pair, separated by $\mathbf{r}_{ij} = \mathbf{r}_j - \mathbf{r}_i$, on the lattice; $J > 0$ is the ferromagnetic exchange coupling, $\mu_0 = 4\pi \times 10^{-7}$ H/m is the vacuum permeability, g is the Landé g-factor, and $\mu_B = 9.274 \times 10^{-24}$ J/T is the Bohr magneton. If necessary, other interactions, anisotropies, and coupling with magnetic fields can be easily included. For example, if one considers a finite model, it is important to include the surface contribution through the demagnetizing field, which vanishes for an ellipsoidal sample with magnetization oriented along a symmetry axis. Slight differences between theoretical and experimental results should be observed if minor effects are disregarded. However, since our main objective is to investigate the dipolar interaction under the SCHA perspective, we consider only bulk interactions in this work. In above equation, \mathbf{S}_i is adopted as a classical dimensionless spin field on the site

i , whose transverse components are written as

$$S_i^x = \sqrt{S^2 - (S_i^z)^2} \cos \varphi_i \quad (2a)$$

$$S_i^y = \sqrt{S^2 - (S_i^z)^2} \sin \varphi_i \quad (2b)$$

In the quantum development, φ_i and S_i^z are promoted to operators that obey the usual commutation relation $[\varphi_i, S_j^z] = i\delta_{ij}$ [16]. Notwithstanding some different procedures in the middle of the process, the final result obtained from the quantum version of the Hamiltonian (1) is the same one obtained from the *a posteriori* quantized Hamiltonian. Therefore, for the sake of simplicity, we will consider classical spin fields for now and leave the quantization to be performed later. Let us define the magnetization along the $\langle 100 \rangle$ direction and consider the fields φ and S^z small enough to perform a series expansion around zero. After expanding up to second order in the φ and S^z fields, the exchange Hamiltonian reads in the momentum space

$$H_{\text{exc}}^{(2)} = \sum_q zJ(1 - \gamma_q)(\rho S^2 \varphi_q \varphi_{-q} + S_q^z S_{-q}^z), \quad (3)$$

where the q -sum extends over the first Brillouin zone. In above equation, the structure factor is defined by

$$\gamma_q = \frac{1}{z} \sum_{\boldsymbol{\eta}} e^{i\mathbf{q} \cdot \boldsymbol{\eta}}, \quad (4)$$

where $\boldsymbol{\eta}$ stands for the nearest neighbor positions, and $z = 6$ is the coordination number for the three-dimensional cubic lattice. In addition, ρ is a renormalization parameter included to take into account higher-order phase fluctuations disregarded in the cosine expansion, which is determined by the self-consistent equation

$$\rho = \left[1 - \frac{\langle (S^z)^2 \rangle_0}{S^2} \right] \exp \left[-\frac{1}{2} \langle \Delta \varphi^2 \rangle_0 \right], \quad (5)$$

where $\Delta \varphi$ is the phase difference between nearest neighbors, and the averages are evaluated by using the harmonic Hamiltonian $H_0 = H_{\text{exc}}^{(2)} + H_{\text{dip}}^{(2)}$. More details about the renormalization parameter are given in Appendix A.

We solve the dipolar interaction following similar steps. First, note that, despite the decaying factor r_{ij}^{-3} , the isotropic contribution is identical to the exchange term, while the anisotropic dipolar contribution is written as

$$\begin{aligned} (\mathbf{S}_i \cdot \mathbf{r}_{ij})(\mathbf{S}_j \cdot \mathbf{r}_{ij}) &= 2z_{ij}y_{ij}\sqrt{S^2 - (S_i^z)^2}S_j^z \sin \varphi_i + \\ &+ \sqrt{S^2 - (S_i^z)^2}\sqrt{S^2 - (S_j^z)^2}(x_{ij}^2 \cos \varphi_i \cos \varphi_j + \\ &+ y_{ij}^2 \sin \varphi_i \sin \varphi_j) + z_{ij}S_i^z S_j^z \end{aligned} \quad (6)$$

where the mixed terms $S_i^x S_j^y$ and $S_i^x S_j^z$ were omitted since they do not yield second-order contributions. We then expand the trigonometric functions as $\cos \varphi \approx$

$1 - \rho_d \varphi^2/2$ and $\sin \varphi \approx \sqrt{\rho_d} \varphi$, where ρ_d is the dipolar

renormalization factor, given by

$$\rho_d = \frac{1}{2} \left[1 - \frac{\langle (S^z)^2 \rangle_0}{S^2} \right] [1 + \exp(-2\langle \varphi^2 \rangle_0)]. \quad (7)$$

Again, the average is determined using the harmonic Hamiltonian and details about the demonstration of the above equation can be found in Appendix (A). Therefore, the quadratic dipolar Hamiltonian is written as

$$H_{\text{dip}}^{(2)} = \frac{\mu_0 (g\mu_B)^2}{4\pi} \sum_{ij} \left[\rho_d S^2 \frac{1}{r_{ij}^3} \left(1 - \frac{3y_{ij}^2}{r_{ij}^2} \right) \varphi_i \varphi_j - \rho_d S^2 \frac{1}{r_{ij}^3} \left(1 - \frac{3x_{ij}^2}{r_{ij}^2} \right) \varphi_i \varphi_i + \frac{1}{r_{ij}^3} \left(1 - \frac{3z_{ij}^2}{r_{ij}^2} \right) S_i^z S_j^z - \frac{1}{r_{ij}^3} \left(1 - \frac{3x_{ij}^2}{r_{ij}^2} \right) S_i^z S_i^z - 6S\sqrt{\rho_d} \frac{z_{ij} y_{ij}}{r_{ij}^2} \varphi_i S_j^z \right] \quad (8)$$

We must be careful with the $q = 0$ limit in performing the Fourier transform, which presents a slow convergence. Only for finite values of q , the result is almost independent of the sample surface. We follow the standard procedures to properly evaluate the lattice sum in $q = 0$ [1, 43]. First, we divide the sum into two regions: one inside a small sphere containing only the nearest sites and the other involving the entire sample outside the small sphere. For the cubic lattice, the sum inside the small sphere vanishes, and the second sum can be converted into a volume integral, which is then written as two surface integrals. The inner surface integral (over the small spherical surface) provides the Lorentz factor $4\pi/3$, while the outer surface results in the demagnetization factor, which depends on the domain shape. Here, we consider an elongated ellipsoid whose major axis is along the magnetization direction, and thereby we can neglect the demagnetizing field. For $q > 0$, the sum can be converted in an integral over the entire domain, which results in the well-known Fourier transform [43]

$$D_{ab}(q) = \sum_r \frac{1}{r^3} \left(\delta_{ab} - \frac{3r_a r_b}{r^2} \right) e^{i\mathbf{q} \cdot \mathbf{r}} = \frac{4\pi}{v_{\text{ws}}} \left(\frac{q_a q_b}{q^2} - \frac{\delta_{ab}}{3} \right) + \mathcal{O}(q^2), \quad (9)$$

where $v_{\text{ws}} = a^3$ is the volume of a cubic Wigner-Seitz cell with edge a (lattice parameter). In momentum space, the quadratic dipolar Hamiltonian is then given by

$$H_{\text{dip}}^{(2)} = \mu_0 \frac{g\mu_B M}{2S} \sum_q \left[\rho_d S^2 \frac{q_y^2}{q^2} \varphi_q \varphi_{-q} + \frac{q_z^2}{q^2} S_q^z S_{-q}^z + 2\sqrt{\rho_d} \frac{q_y q_z}{q^2} \varphi_q S_{-q}^z \right], \quad (10)$$

where $M = g\mu_B S/v_{\text{ws}}$ is the magnetization. Note that there is no dependence on q_x and the dipolar contribution vanishes for vector momentum along the $\langle 100 \rangle$

direction (considered as the preferred magnetization direction). This implies that along the magnetization direction, spin-waves have lower energy since there is no effective dipolar field influence in this direction.

A. Semiclassical approach

Before we quantize the Hamiltonian, let us analyze the semiclassical limit. Gathering both exchange and dipolar contributions, we obtain the harmonic Hamiltonian

$$H_0 = \sum_q [S^2 A_q \varphi_q \varphi_{-q} + B_q S_q^z S_{-q}^z + S C_q \varphi_q S_{-q}^z], \quad (11)$$

where we have defined the coefficients

$$A_q = zJ\rho(1 - \gamma_q) + J_d \rho_d \sin^2 \theta_q \cos^2 \phi_q \quad (12a)$$

$$B_q = zJ(1 - \gamma_q) + J_d \sin^2 \theta_q \sin^2 \phi_q \quad (12b)$$

$$C_q = 2J_d \sqrt{\rho_d} \sin^2 \theta_q \sin \phi_q \cos \phi_q, \quad (12c)$$

with $J_d = (\mu_0 g\mu_B M)/2S$. In addition, θ_q and ϕ_q are the polar and azimuth angles between \mathbf{q} and the preferred magnetization direction, defined by $q_y = q \sin \theta_q \cos \phi_q$ and $q_z = q \sin \theta_q \sin \phi_q$. Note that momentum components appear only in a quadratic form in the Hamiltonians (3) and (10). Hence, the A_q , B_q , and C_q coefficients are symmetric under the replacement $\mathbf{q} \rightarrow -\mathbf{q}$. As expected, the dipolar energy vanishes along the magnetization direction and reaches its maximum for $\theta_q = \pi/2$. The spin-wave dynamics is obtained from the Hamilton equations

$$\hbar \dot{S}_q^z = -\frac{\partial H_0}{\partial \varphi_q} = -2S A_q S_q^y - S C_q S_q^z \quad (13)$$

$$\hbar \dot{S}_q^y = S \frac{\partial H_0}{\partial S_q^z} = 2S B_q S_q^z + S C_q S_q^y, \quad (14)$$

where we use $S_q^y \approx S\varphi_q$. Thus, considering solutions in the form of harmonic travelling spin-waves with temporal dependence proportional to $\exp(i\omega_q t)$, we obtain the system of linear equations involving the transverse components

$$\begin{pmatrix} i\hbar\omega_q - SC_q & -2SB_q \\ 2SA_q & i\hbar\omega + SC_q \end{pmatrix} \begin{pmatrix} S_q^y \\ S_q^z \end{pmatrix} = 0, \quad (15)$$

which provides the spin-wave energy

$$E_q = \hbar\omega_q = S\sqrt{4A_qB_q - C_q^2}. \quad (16)$$

For the pure exchange Hamiltonian, it is easy to verify that $E_q = 2SJz\sqrt{\rho}(1 - \gamma_q)$, and so we can define the renormalized exchange coupling as $J_r(T) = \sqrt{\rho(T)}J$. For the dipolar model, it is not possible to exactly factorize the expression and obtain the same result; however, since $\rho \approx \rho_d$, we can still use $J_r(T)$ as an approximated result.

Using the harmonic Hamiltonian given by Eq. (11), we can evaluate the required statistical averages for determining the renormalization factors, to wit

$$\langle S_q^z S_{-q}^z \rangle_0 = \frac{2S^2 A_q}{\beta E_q^2} \quad (17)$$

and

$$\langle \varphi_q \varphi_{-q} \rangle_0 = \frac{2B_q}{\beta E_q^2}, \quad (18)$$

with $\beta = (k_B T)^{-1}$. In above equations, we extend the limit of integration to $\pm\infty$ due to the fast decreasing of $\exp(-\beta H_0)$ at low temperatures. The distributions in the partition function are then treated as Gaussian.

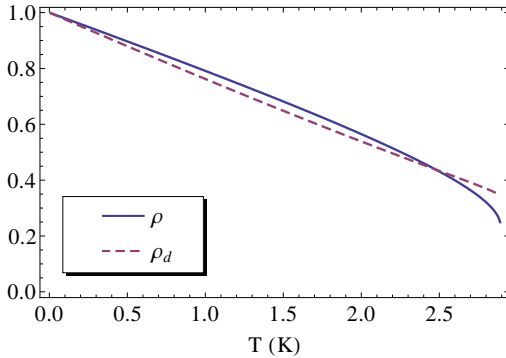


FIG. 1. The renormalization factors for $S = 1$, $J/k_B = 1$ K, and $J_d = 0.1J$. At $T_c = 2.90$ K, ρ abruptly drops to zero while ρ_d assumes a finite value.

The renormalization parameters are determined by solving the ρ and ρ_d equations self-consistently. In general, the convergence is very fast and are required few iterations to reach the solution. At the zero-temperature limit, it is easy to verify that ρ and ρ_d tend to one, as

one sees in Fig. (1), which allows to simplify the energy equation and obtain the spin-wave dispersion relation

$$\omega_q = \frac{2JSz}{\hbar}(1 - \gamma_q) \left[1 + \frac{\hbar\omega_M \sin^2 \theta_q}{2JSz(1 - \gamma_q)} \right]^{1/2}, \quad (19)$$

where $\omega_M = g\mu_B\mu_0 M$. The above outcome coincides with the well-known result for a ferromagnetic insulator with dipolar interaction [41]. Indeed, one can determine the dispersion relation by using the Landau-Lifschitz equation $\dot{\mathbf{M}} = -\gamma\mu_0 \mathbf{M} \times \mathbf{H}_{\text{eff}}$, where the effective field $\mathbf{H}_{\text{eff}} = \mathbf{H}_{\text{exc}} + \mathbf{H}_{\text{dip}}$. In the Fourier space, the exchange and dipolar fields [considering the magnetostatic limit for which $\nabla \cdot (\mathbf{M} + \mathbf{H}_{\text{dip}}) = 0$, and $\nabla \times \mathbf{H}_{\text{dip}} = \mathbf{0}$] are respectively given by $\mathbf{H}_{\text{exc}} = z\kappa\mathbf{M}_q - \kappa(aq)^2\mathbf{M}_q^\perp$, and $\mathbf{H}_{\text{dip}} = -(\hat{\mathbf{q}} \cdot \mathbf{M}_q^\perp)\hat{\mathbf{q}}$, where the transverse magnetization is $\mathbf{M}_q^\perp = \mathbf{M}_q^y + \mathbf{M}_q^z$, and $\kappa = 2JS/\hbar\omega_M$. Note that we have considered a uniform longitudinal magnetization component and the vector \mathbf{q} was defined as previously. Adopting the oscillating time behavior for the magnetization, $\mathbf{M}_q(t) = \mathbf{M}_q(0)e^{i\omega_q t}$, the Landau-Lifschitz equation yields

$$\omega_q = \frac{2JSq^2}{\hbar} \left[1 + \frac{\hbar\omega_M \sin^2 \theta_q}{2JSq^2} \right]^{1/2}, \quad (20)$$

which is the long wavelength limit of Eq. (19). Considering $S = 1$, $J/k_B = 1$ K, and $J_d/k_B = 0.1$ K, we determine the critical temperature (the point in which ρ abruptly vanishes) at $T_c = 2.90$ K. Opposite to the exchange renormalization factor, ρ_d is finite at T_c . For $T > 0$, the renormalization factors are slightly different; however, for $T \lesssim 0.9T_c$, $\rho \approx \rho_d$ and the dispersion relation can be written as $\omega_q(T) \approx \sqrt{\rho(T)}\omega_q(T=0)$.

The magnetization along the $\langle 100 \rangle$ direction is readily determined and given by

$$\langle S^x \rangle = S - \frac{1}{N} \sum_q \left(\frac{1}{2S} \langle S_q^z S_{-q}^z \rangle_0 + \frac{S}{2} \langle \varphi_q \varphi_{-q} \rangle_0 \right), \quad (21)$$

while $\langle S^z \rangle$ and $\langle S^y \rangle$ are null.

B. Quantum Hamiltonian

Although the semiclassical results are in reasonable agreement with the literature, we can get better outcomes through the quantized Hamiltonian. To perform the quantization of the spin-waves, we promote the fields φ_q and S_q^z to operators that satisfy $[\varphi_q, S_{q'}^z] = i\delta_{qq'}$. Therefore, it is convenient to define the bosonic operators a_q expressed by

$$\varphi_q = \frac{1}{\sqrt{2S}}(a_q^\dagger + a_{-q}) \quad (22a)$$

$$S_q^z = \frac{i\sqrt{S}}{\sqrt{2}}(a_q^\dagger - a_{-q}), \quad (22b)$$

which leads to

$$H_0 = \sum_q \frac{S}{2} \left[(A_q + B_q)(a_q^\dagger a_q + a_{-q} a_{-q}^\dagger) + (A_q - B_q + iC_q)a_q^\dagger a_{-q}^\dagger + (A_q + B_q - iC_q)a_{-q} a_q \right]. \quad (23)$$

The diagonalization is obtained from the definition of new bosonic operators by the Bogoliubov transform

$$a_q = e^{i\psi_q/2} \cosh \chi_q \alpha_{-q} + e^{i\psi_q/2} \sinh \chi_q \alpha_q^\dagger, \quad (24)$$

where χ_q is established by the relation

$$\tanh \chi_q = -\frac{|A_q - B_q + iC_q|}{A_q + B_q} \quad (25)$$

and ψ_q is the phase of $(A_q - B_q + iC_q)$. Therefore, after a straightforward procedure, we obtain

$$H_0 = \sum_q \hbar \omega_q \left(\alpha_q^\dagger \alpha_q + \frac{1}{2} \right), \quad (26)$$

where the spin-wave energy is again given by the relation $\hbar \omega_q = \tilde{S} \sqrt{4A_q B_q - C_q^2}$, and we replace the classical spin value S by $\tilde{S} = \sqrt{S(S+1)}$.

The renormalization parameters are calculated using the same Eqs. (5) and (7) but the averages are determined by using the quantum harmonic Hamiltonian. Through the relation between spin and bosonic operators, as well as the Bogoliubov transform, we are able to achieve

$$\langle \varphi_q \varphi_{-q} \rangle_0 = \frac{B_q}{E_q} \coth \left(\frac{\beta E_q}{2} \right) \quad (27)$$

and

$$\langle S_q^z S_{-q}^z \rangle_0 = \frac{S^2 A_q}{E_q} \coth \left(\frac{\beta E_q}{2} \right). \quad (28)$$

Note that, in the small energy limit, *i.e.*, $E_q \ll k_B T$, we approximate $\coth(\beta E_q/2)$ by $2/\beta E_q$, and the semiclassical averages are recovered.

Fig. (2) shows the temperature dependence of the renormalization factors. Due to the replacement of S by \tilde{S} , we observe an increasing in the critical temperature, from $T_c = 2.90$ K to $T_c = 4.78$ K. As we will see in the next section, the quantum results better agree with experimental measures. In addition, as one can see, $\rho_d \gtrsim \rho$, and both parameters are smaller than the respective semiclassical results. As expected, magnons have a more expressive contribution to disorder the magnetic phase in the quantum limit.

The effect of the dipolar interaction on the critical temperature is shown in Fig. (3). Using the semiclassical approach, we obtain T_c almost constant for $0 \leq J_d \leq J$, while for the quantum analysis, T_c is a slightly increasing function of J_d . Despite the small correction, the dipolar interaction is important to determine the transition temperature in Europium Chalcogenides with more precision, as demonstrated in the next section.

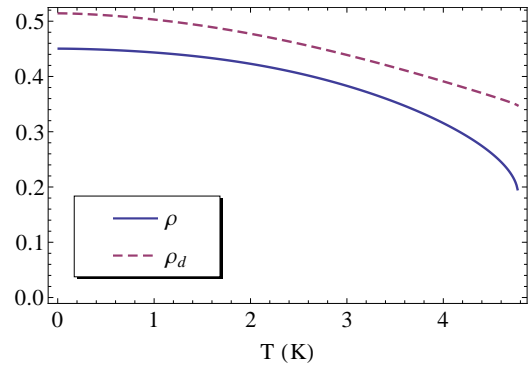


FIG. 2. The renormalization factors for $\tilde{S} = \sqrt{2}$, $J/k_B = 1$ K, and $J_d = 0.1J$. Here, the critical temperature is given by $T_c = 4.78$ K.

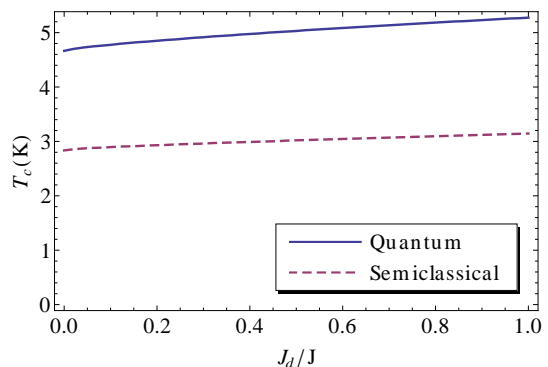


FIG. 3. The critical temperature as function of the dipolar interaction intensity.

III. EUROPIUM CHALCOGENIDES

To verify the effectiveness of the SCHA including dipolar interactions, we apply the formalism to determine the energy spectrum and transition temperature of Europium Oxide (EuO) and Europium Sulfite (EuS), two ferromagnetic insulators with well-known properties [42, 44–52].

The Europium Chalcogenides present a bulk with a high degree of symmetry that makes them ideal to be described by the Heisenberg Hamiltonian. The magnetic properties arise from Eu^{2+} ions that exhibit spin $S = 7/2$ and orbital angular momentum $L = 0$. Because of the highly localized wave-function of the 4f electrons, the exchange coupling between Eu^{2+} ions occurs due to indirect exchange with unoccupied 5d conduction bands and superexchange coupling [44]. The Europium ions are localized in an fcc lattice with isotropic exchange interaction between nearest and near-nearest neighbors as well as long-range dipolar interaction. Neither the exchange nor the dipolar interaction shows a preferred magnetization direction; however, a small anisotropy from the crystalline field orients the spin on the direction $\langle 111 \rangle$. Note that the Heisenberg Hamiltonian and the isotropic part of the dipolar interaction are invariant under ro-

tations, and they show the same structure whether we orient the magnetization in $\langle 100 \rangle$ or $\langle 111 \rangle$ directions. On the other hand, we must take care of the anisotropic part of the dipolar interaction when we rotate the preferred magnetization axis. Here, we work with directions according to the fcc lattice, and the anisotropic part of the dipolar interaction is adjusted to this frame (initially it is written in such a way that the x-axis coincides with the $\langle 111 \rangle$ direction and later it is rotated to a new frame where the x-axis coincides with the $\langle 100 \rangle$ direction). The Hamiltonian is written as

$$H = -J_1 \sum_{\langle ij \rangle} \mathbf{S}_i \cdot \mathbf{S}_j - J_2 \sum_{\langle\langle ij \rangle\rangle} \mathbf{S}_i \cdot \mathbf{S}_j + \frac{\mu_0 (g\mu_B)^2}{4\pi} \sum_{ij} \left[\frac{\mathbf{S}_i \cdot \mathbf{S}_j}{r_{ij}^3} - 3 \frac{(\mathbf{S}_i \cdot \mathbf{r}_{ij})(\mathbf{S}_j \cdot \mathbf{r}_{ij})}{r_{ij}^5} \right], \quad (29)$$

where J_1 and J_2 represent the exchange coupling between nearest (nn) and near-nearest (nnn) neighbors, respectively. For EuO ($a = 5.141 \text{ \AA}$), we adopt $J_1/k_B = 0.606 \text{ K}$ and $J_2/k_B = 0.119 \text{ K}$, while $J_1/k_B = 0.236 \text{ K}$ and $J_2/k_B = -0.118 \text{ K}$ are the exchange couplings for EuS ($a = 5.960 \text{ \AA}$) [46]. Using the SCHA, we obtain a harmonic Hamiltonian similar to the Eq. (11); however, the coefficients are now given by

$$A_q = z_1 J_1 \rho_1 (1 - \gamma_q^{(nn)}) + z_2 J_2 \rho_2 (1 - \gamma_q^{(nnn)}) + J_d \rho_d \sin^2 \theta_q \cos^2 \phi_q \quad (30a)$$

$$B_q = z_1 J_1 (1 - \gamma_q^{(nn)}) + z_2 J_2 \rho (1 - \gamma_q^{(nnn)}) + J_d \sin^2 \theta_q \sin^2 \phi_q \quad (30b)$$

$$C_q = 2J_d \sqrt{\rho_d} \sin^2 \theta_q \sin \phi_q \cos \phi_q, \quad (30c)$$

where the coordination numbers are $z_1 = 12$ and $z_2 = 6$, and the structure factors are

$$\gamma_1^{(nn)} = \frac{1}{6} \left[\cos\left(\frac{q_x}{2}\right) \cos\left(\frac{q_y}{2}\right) + \cos\left(\frac{q_y}{2}\right) \cos\left(\frac{q_z}{2}\right) + \cos\left(\frac{q_z}{2}\right) \cos\left(\frac{q_x}{2}\right) \right], \quad (31a)$$

$$\gamma_q^{(nnn)} = \frac{1}{3} (\cos q_x + \cos q_y + \cos q_z). \quad (31b)$$

The angles θ_q and ϕ_q are defined in relation to the magnetization preferred axis ($\langle 111 \rangle$ direction) and, in the reference frame used to define $\gamma_q^{(nn)}$ and $\gamma_q^{(nnn)}$, we have

$$\cos \theta_q = \frac{q_x + q_y + q_z}{\sqrt{3}q}, \quad \tan \phi_q = \frac{q_x + q_y - 2q_z}{\sqrt{3}(q_x - q_y)}. \quad (32)$$

Here, we consider three renormalization factors, again evaluated using Eqs. (5) and (7), one for each contribution of the Hamiltonian. For the exchange coupling, the structure factor γ_q is chosen according to the nn or nnn interaction. As in the pure exchange Hamiltonian, we define the renormalized coupling terms by $J_1(T) = \sqrt{\rho_1(T)} J_1(0)$ and $J_2(T) = \sqrt{\rho_2(T)} J_2(0)$, which reproduce very well the result obtained from Dyson-Maleev representation for EuO [48] and EuS [50]. Both

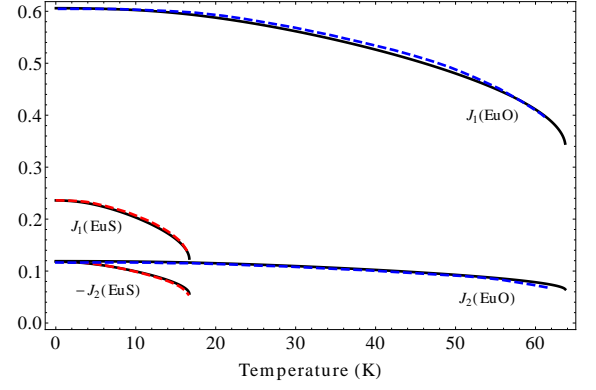


FIG. 4. The renormalized coupling J_1 and J_2 (in units of k_B) as function of temperature for EuO and EuS. The black solid lines are the SCHA results, the dashed red line is from Ref. [48], and the dashed blue line is from Ref. [50]

quantum SCHA and Dyson-Maleev results are shown in Fig. (4). The solid line ends at the critical temperature (the point where the renormalization parameter abruptly vanishes), very close to the Curie temperature. Applying the quantum SCHA, we obtain $T_c = 63.75 \text{ K}$ for EuO and $T_c = 16.71 \text{ K}$ for EuS, while the experimental values of the Curie temperatures are $T_C = 69.15 \text{ K}$ (EuO) and $T_C = 16.57 \text{ K}$ (EuS) [46]. The transition temperatures evaluated from both semiclassical and quantum SCHA for the pure exchange Hamiltonian and the full model, including dipolar interaction, are listed in Table (III). As one can see, we reach the best results by using the quantum SCHA including the dipolar interaction.

Using the SCHA formalism, we also evaluate the spin-wave dispersion at $T = 5.5 \text{ K}$ to compare with neutron scattering experiments [46]. Fig. (5) shows the curves (solid lines) calculated through SCHA and the experimental data for EuO and EuS. In both cases, the SCHA provides good agreement with the experiments. In addition, Fig. (6) shows the temperature dependence of the reduced magnetization for both EuO (in blue) and EuS (in red). The figure plots the data from neutron scattering experiments [47] (following the same color scheme). For EuS (EuO), the calculated magnetization is slightly smaller (larger) than the experimental measurements. The experimental measurements were done using thin-slab samples obtained from polycrystalline powders [46]. Surface effects, which were disregarded in our analysis, could justify the slight difference between the theoretical and experimental results. For the same reason, one could justify the difference between the SCHA and experimental critical temperature, mainly for EuO. Since exchange couplings are intrinsic properties, depending on the superposition of electron wave-functions, surface contributions are negligible for the renormalized coupling J_1 and J_2 , which explain the good agreement in Fig. (4). On the other hand, D. A. Garanin applied the SCGA with a simplified dipolar interaction to obtain a critical

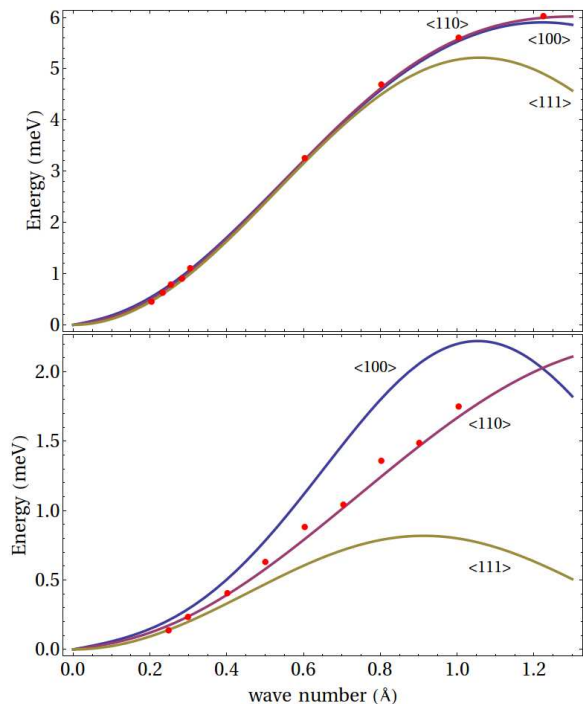


FIG. 5. Spin-wave dispersion relation (at $T = 5.5$ K) for EuO (above) and EuS (below). The solid lines are results of the SCHA formalism, and the red points are neutron scattering measures along the $\langle 110 \rangle$ direction extracted from Ref. [46].

Method	EuO	EuS
Pure exchange, semiclassical SCHA	48.64 K	17.64 K
Pure exchange, quantum SCHA	61.24 K	15.22 K
Full model, semiclassical SCHA	50.60 K	19.49 K
Full model, quantum SCHA	63.75 K	16.71 K
Experimental data [46]	69.15 K	16.57 K

TABLE I. Transition temperature obtained from SCHA considering pure exchange Hamiltonian and including dipolar interaction. Both semiclassical and quantum are considered and the best result is obtained by using the quantum SCHA with dipolar interaction.

temperature $T_c \approx 69$ K for the EuO [19]. At the same time, the magnetization obtained by Garanin is slightly larger than the experimental data, as the SCHA result. Therefore, more investigation is necessary to explain the slightly lower EuO critical temperature obtained from SCHA.

IV. SUMMARY AND CONCLUSIONS

The SCHA method is an efficient formalism for treating spin models at finite temperature, provided that the method deals with simple harmonic Hamiltonians. The temperature dependence is included through renormalization parameters that need to be solved by self-consistent equations. The SCHA has been used for many

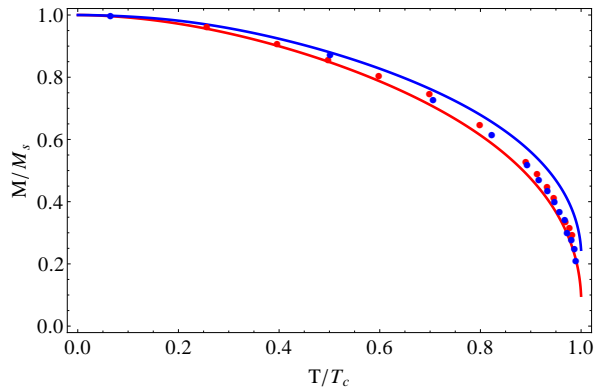


FIG. 6. The reduced magnetization curve as function of relative temperature T/T_c (EuO in blue and EuS in red). The solid lines are the SCHA results and the points were obtained for neutron scattering experiments [47]

years, mainly to determine critical temperatures; however, in general, only short-range interaction has been considered. Since dipolar interaction is a relevant contribution for many magnetic experiments, we developed the SCHA to include the dipolar field.

Using the SCHA, we obtained the spin-wave spectrum energy, the transition temperature, renormalized couplings, and magnetization, while other results can also be easily determined. The SCHA results coincide with theoretical development obtained from standard bosonic representations in the zero-temperature limit. To verify our equations, we applied the formalism to the ferromagnetic Europium Chalcogenides: EuO and EuS. The results were compared with well-known results obtained from usual bosonic representations and neutron scattering experiments. We achieved a good agreement for both materials, mainly for Europium Sulfite. For EuS, the transition temperature provided by SCHA (16.71 K) showed an error of less than 1 percent when compared to the experimental value (16.57 K). Besides, the theoretical magnetization curve presented an excellent fit with the neutron scattering data. In the EuO case, the determined transition temperature was $T_c = 63.75$ K, while the experimental result is given by $T_c = 69.15$ K. It is known that anisotropic energy provides a small gap of the order of $3.5 \mu\text{eV}$ in EuO (and one order of magnitude smaller in EuS) that was disregarding in our work. However, this anisotropy is insufficient to explain the observed difference. In addition, surface effects, which were also disregarded, could contribute to the small difference between theoretical and experimental results. The calculated magnetization curve is precise at the low-temperature limit, but SCHA gives results slightly different from the experimental data for $T \gtrsim 0.5T_c$ (approximately 10% larger at $T = 0.9T_c$, for EuO). Finally, the renormalized exchange coupling evaluated by SCHA for both materials showed an excellent agreement with the literature.

The SCHA revealed a great formalism in describing the magnetic thermodynamics in models endowed with dipo-

lar interaction. Likewise the usual bosonic formalisms, the SCHA method can be applied in the theoretical investigation of magnetism in various fields. Since the SCHA formalism is a quadratic model, its application is more manageable than traditional bosonic representations that need to include spin-wave interaction to consider corrections of fourth-order or higher. In addition, the SCHA shows some advantages compared with the SCGA, which is another method with similar purposes. The first one is related to the smaller number of required self-consistent parameters. For example, for the isotropic ferromagnetic Heisenberg model in the presence of a field H^z , the SCHA requires only a parameter (the renormalization term ρ) to determine the thermodynamics. At the same time, SCGA needs three self-consistent unknown variables (the magnetization and the longitudinal and transverse components of the mean-field fluctuation) to treat the same Hamiltonian. The difference in self-consistent parameters between both methods is even more significant for more general Hamiltonians. Another advantage refers to the quantization procedure. Whereas the SCGA applies to only classical spin models, the SCHA Hamiltonian, which is written in terms of S^z and φ , can be easily quantized by imposing the commutation relation $[\varphi_i, S_j^z] = i\delta_{ij}$. Finally, despite the excellent SCGA results, it is easier to implement the dipolar interaction in the SCHA than in the SCGA, which could be a decisive point depending on the problem addressed.

Appendix A: Renormalization factors

The dynamics of S^z depends on which Hamiltonian is used to determine the time derivative, and the result is strongly affected whether one uses the simple harmonic Hamiltonian (without any correction) or the complicated full version. Therefore, we include the renormalization parameter in the quadratic Hamiltonian to improve the results without turning the evaluation overly laborious.

In order to determine the renormalization factors, we compare the average $\langle \dot{S}_q^z \dot{S}_{-q}^z \rangle_0$ evaluated using the quadratic Hamiltonian H_0 , given by Eq. (11), with the result obtained from the full Hamiltonian H , *i.e.* $\langle \dot{S}_q^z \dot{S}_{-q}^z \rangle$. Starting with the former, we obtain

$$\begin{aligned} \hbar^2 \langle \dot{S}_q^z \dot{S}_{-q}^z \rangle_0 &= 4S^4 A_q^2 \langle \varphi_q \varphi_{-q} \rangle_0 + 4S^3 A_q C_q \langle \varphi_q S_{-q}^z \rangle_0 + \\ &+ S^2 C_q^2 \langle S_q^z S_{-q}^z \rangle_0 = \frac{2S^2 A_q}{\beta}. \end{aligned} \quad (\text{A1})$$

To find out the second term, given by the Fourier transform

$$\langle \dot{S}_q^z \dot{S}_{-q}^z \rangle = \frac{1}{N} \sum_{ij} \langle \dot{S}_i^z \dot{S}_j^z \rangle e^{i\mathbf{q} \cdot (\mathbf{r}_j - \mathbf{r}_i)}, \quad (\text{A2})$$

we use the following useful relation, obtained after an

integration by parts,

$$\begin{aligned} \hbar^2 \langle \dot{S}_i^z \dot{S}_j^z \rangle &= \frac{1}{Z} \int \mathcal{D}\varphi \mathcal{D}S^z \frac{\partial H}{\partial \varphi_i} \frac{\partial H}{\partial \varphi_j} e^{-\beta H} \\ &= \frac{1}{Z} \int \mathcal{D}\varphi \mathcal{D}S^z \frac{1}{\beta} \frac{\partial^2 H}{\partial \varphi_i \partial \varphi_j} e^{-\beta H}, \end{aligned} \quad (\text{A3})$$

where Z is the partition function, and the integration measure $\mathcal{D}\varphi \mathcal{D}S^z$ stands for the field integration over each site on the lattice. In addition, we extend the integration limit to $-\infty < \varphi, S^z < \infty$ and so we will deal with Gaussian integrals. Since the exchange and dipolar Hamiltonians are decoupled, we can develop them separately. For the exchange term, we get

$$\frac{\partial^2 H_{\text{exc}}}{\partial \varphi_i \partial \varphi_j} = 2 \sum_{\eta} h_{i\eta}^{\text{exc}} (\delta_{j\eta} - \delta_{ij}), \quad (\text{A4})$$

with $h_{ij}^{\text{exc}} = -J \sqrt{S^2 - (S_i^z)^2} \sqrt{S^2 - (S_j^z)^2} \cos(\varphi_i - \varphi_j)$ and η being the nearest neighbors. Then, the Fourier transform yields

$$\hbar^2 \langle \dot{S}_q^z \dot{S}_{-q}^z \rangle_{\text{exc}} = \frac{2zJ}{\beta} (1 - \gamma_q) \langle h^{\text{exc}} \rangle_0, \quad (\text{A5})$$

where we assume that $\langle h^{\text{exc}} \rangle_0$ is independent of the site position and the average is determined through the harmonic Hamiltonian H_0 . We can evaluate the averages over S^z and φ independently for decoupled fields. However, in our case, the Hamiltonian present mixed terms and, in space coordinates, it looks like

$$H_0 = \sum_{ij} [S^2 A_{ij} \varphi_i \varphi_j + B_{ij} S_i^z S_j^z + S C_{ij} \varphi_i S_j^z]. \quad (\text{A6})$$

Then, some extra steps are necessary to properly determine $\langle h^{\text{exc}} \rangle_0$. Firstly, we consider that $S_i^z \approx S_j^z \ll S$ and write $\langle h^{\text{exc}} \rangle_0 = S^2 \langle (1 - s^z) \cos \phi \rangle$, where $s^z = S^z/S$ and $\phi = \Delta\varphi$. Since we are dealing with Gaussian integrals, we can replace $\langle \cos \phi \rangle_0$ by $\exp(-\langle \phi^2 \rangle_0/2)$. Now, to determine the average $\langle (s^z)^2 \cos \phi \rangle_0$, we expand the cosine function and apply the general result for Gaussian distributions, for example, in the variables x and y

$$\langle x^{2m} y^{2n} \rangle = \sum_{p=0}^{\min(m,n)} c_{mnp} \langle x^2 \rangle^{m-p} \langle y^2 \rangle^{n-p} \langle xy \rangle^{2p}, \quad (\text{A7})$$

whose coefficients are given by

$$c_{mnp} = \frac{(2m)!(2n)!(2m-2p-1)!!(2n-2p-1)!!}{(2m-2p)!(2n-2p)!(2p)!} \quad (\text{A8})$$

Therefore, it is a straightforward procedure to get the exact result

$$\langle (s^z)^2 \cos \phi \rangle_0 = [\langle (s^z)^2 \rangle_0 - \langle s^z \phi \rangle_0^2] \exp \left[-\frac{\langle \phi^2 \rangle_0}{2} \right] \quad (\text{A9})$$

and disregarding the forth-order term $\langle s^z \phi \rangle_0^2$, we obtain Eq. (5). Note that, in the decoupled fields case, we have

$\langle s^z \varphi \rangle_0 = 0$, which provides the result obtained from the relation $\langle (s^z)^2 \cos \phi \rangle_0 = \langle (s^z)^2 \rangle_0 \langle \cos \phi \rangle_0$. In addition, one can use the same approach to implement higher-order contributions to the SCHA renormalization parameter, although the corrections are minor and do not provide reasonable changes in final results. The more relevant contribution to determining the transition temperature comes from the exponential term.

The dipolar renormalization parameter follows the same development. Considering the isotropic part and the terms present in Eq. (6), the derivative of the dipolar Hamiltonian reads

$$\frac{\partial^2 H_{\text{dip}}}{\partial \varphi_i \partial \varphi_j} = \frac{J_d v_{\text{ws}}}{4\pi} \sum_{\eta} \left[2\xi_{i\eta}^{xx} (\delta_{j\eta} \sin \varphi_i \sin \varphi_{\eta} - \delta_{ij} \cos \varphi_i \cos \varphi_{\eta}) + 2\xi_{i\eta}^{yy} (\delta_{j\eta} \cos \varphi_i \cos \varphi_{\eta} - \delta_{ij} \sin \varphi_i \sin \varphi_{\eta}) - \xi_{i\eta}^{yz} \sin \varphi_i \delta_{ij} \right], \quad (\text{A10})$$

where η now represents any site on the lattice, not only the nearest neighbors as previously, and the ξ coefficients

are expressed by

$$\begin{aligned} \xi_{ij}^{xx} &= \sqrt{S^2 - (S_i^z)^2} \sqrt{S^2 - (S_j^z)^2} \left(\frac{1}{r_{ij}^3} - \frac{3x_{ij}^2}{r_{ij}^5} \right), \\ \xi_{ij}^{yy} &= \sqrt{S^2 - (S_i^z)^2} \sqrt{S^2 - (S_j^z)^2} \left(\frac{1}{r_{ij}^3} - \frac{3y_{ij}^2}{r_{ij}^5} \right), \\ \xi_{ij}^{yz} &= -6 \sqrt{S^2 - (S_i^z)^2} S_j^z \frac{y_{ij} z_{ij}}{r_{ij}^5}. \end{aligned} \quad (\text{A11})$$

For determining the averages of above equation, we make the same previous considerations. Besides, we adopt that the sine terms are much smaller than the cosine ones, provided that $\varphi \ll 1$. In performing the Fourier transform, we obtain

$$\hbar^2 \langle \dot{S}_q^z \dot{S}_{-q}^z \rangle_{\text{dip}} = \frac{2J_d}{\beta} \langle (S^2 - (S^z)^2) \cos^2 \varphi \rangle_0 \frac{q_y^2}{q^2}, \quad (\text{A12})$$

and comparing with $\hbar^2 \langle \dot{S}_q^z \dot{S}_{-q}^z \rangle_0$, we see that the dipolar renormalization parameter is given by

$$\rho_d = \left\langle \left(1 - \frac{(S^z)^2}{S^2} \right) \cos^2 \varphi \right\rangle_0. \quad (\text{A13})$$

After a fast algebraic manipulation, and using the same procedures of the exchange case, we finally obtain Eq. (7). Other cases, as the near-nearest exchange interaction in the Europium Chalcogenides, are solved following the same steps presented here.

-
- [1] T. Holstein and H. Primakoff, *Physical Review* **58**, 1098 (1940).
 - [2] A. Auerbach, *Interacting electrons and quantum magnetism* (Springer Science & Business Media, 2012).
 - [3] D. P. Arovas and A. Auerbach, *Physical Review B* **38**, 316 (1988).
 - [4] S. Sarker, C. Jayaprakash, H. R. Krishnamurthy, and M. Ma, *Physical Review B* **40**, 5028 (1989).
 - [5] A. Auerbach and D. P. Arovas, *Journal of Applied Physics* **67**, 5734 (1990).
 - [6] M. D. Stiles and A. Zangwill, *Physical Review B* **66**, 014407 (2002).
 - [7] A. E. Trumper, L. O. Manuel, C. J. Gazza, and H. A. Ceccatto, *Physical review letters* **78**, 2216 (1997).
 - [8] M. G. Gonzalez, E. A. Ghioldi, C. J. Gazza, L. O. Manuel, and A. E. Trumper, *Physical Review B* **96**, 174423 (2017).
 - [9] E. A. Ghioldi, M. G. Gonzalez, S.-S. Zhang, Y. Kamiya, L. O. Manuel, A. E. Trumper, and C. D. Batista, *Physical Review B* **98**, 184403 (2018).
 - [10] S.-S. Zhang, E. A. Ghioldi, Y. Kamiya, L. O. Manuel, A. E. Trumper, and C. D. Batista, *Physical Review B* **100**, 104431 (2019).
 - [11] R. Rajaraman, (1982).
 - [12] N. Nagaosa, *Quantum field theory in condensed matter physics* (Springer Science & Business Media, 2013).
 - [13] D. Garanin, *Physical Review B* **53**, 11593 (1996).
 - [14] G. Horwitz and H. B. Callen, *Physical Review* **124**, 1757 (1961).
 - [15] R. Stinchcombe, G. Horwitz, F. Englert, and R. Brout, *Physical Review* **130**, 155 (1963).
 - [16] J. Villain, *Journal de Physique* **35**, 27 (1974).
 - [17] A. S. T. Pires, A. R. Pereira, and M. E. Gouvêa, *Physical Review B* **49**, 9663 (1994).
 - [18] A. Pires, *Physics Letters A* **202**, 309 (1995).
 - [19] A. R. Pereira, A. S. T. Pires, and M. E. Gouvea, *Physical Review B* **51**, 16413 (1995).
 - [20] B. V. Costa, A. R. Pereira, and A. S. T. Pires, *Physical Review B* **54**, 3019 (1996).
 - [21] A. S. T. Pires, *Solid State Communications* **104**, 771 (1997).
 - [22] M. E. Gouvêa, G. M. Wysin, S. A. Leonel, A. S. T. Pires, T. Kampeter, and F. G. Mertens, *Physical Review B* **59**, 6229 (1999).
 - [23] S. Menezes, M. Gouvêa, and A. S. T. Pires, *Physics Letters A* **166**, 330 (1992).
 - [24] A. S. T. Pires and M. E. Gouvea, *Physical Review B* **48**, 12698 (1993).
 - [25] A. S. T. Pires, *Physical Review B* **50**, 9592 (1994).
 - [26] A. Pires, *Solid state communications* **100**, 791 (1996).
 - [27] A. S. T. Pires, *Physical Review B* **53**, 235 (1996).
 - [28] A. S. T. Pires, *Physical Review B* **54**, 6081 (1996).

- [29] A. Pires, Solid state communications **112**, 705 (1999).
- [30] A. S. T. Pires and M. Gouvêa, The European Physical Journal B-Condensed Matter and Complex Systems **44**, 169 (2005).
- [31] M. Gouvêa and A. Pires, physica status solidi (b) **242**, 2138 (2005).
- [32] A. S. T. Pires, B. V. Costa, and R. A. Dias, Physical Review B **78**, 212408 (2008).
- [33] A. Pires, Journal of Magnetism and Magnetic Materials **452**, 315 (2018).
- [34] A. Pires, Physica A: Statistical Mechanics and its Applications **373**, 387 (2007).
- [35] A. Pires, L. Lima, and M. Gouvea, Journal of Physics: Condensed Matter **20**, 015208 (2007).
- [36] A. Pires and M. Gouvea, Physica A: Statistical Mechanics and its Applications **388**, 21 (2009).
- [37] A. Pires and B. Costa, Physica A: Statistical Mechanics and its Applications **388**, 3779 (2009).
- [38] A. R. Moura, A. S. Pires, and A. R. Pereira, Journal of magnetism and magnetic materials **357**, 45 (2014).
- [39] A. Moura and R. Lopes, Journal of Magnetism and Magnetic Materials **472**, 1 (2019).
- [40] A. Moura, Journal of magnetism and magnetic materials **369**, 62 (2014).
- [41] S. M. Rezende, *Fundamentals of Magnonics*, Vol. 969 (Springer, 2020).
- [42] P. Wachter, Handbook on the physics and chemistry of rare earths **2**, 507 (1979).
- [43] M. H. Cohen and F. Keffer, Physical Review **99**, 1128 (1955).
- [44] T. Kasuya, IBM Journal of Research and Development **14**, 214 (1970).
- [45] O. Dietrich, A. Henderson Jr, and H. Meyer, Physical Review B **12**, 2844 (1975).
- [46] L. Passell, O. Dietrich, and J. Als-Nielsen, Physical Review B **14**, 4897 (1976).
- [47] J. Als-Nielsen, O. Dietrich, and L. Passell, Physical Review B **14**, 4908 (1976).
- [48] O. Dietrich, J. Als-Nielsen, and L. Passell, Physical Review B **14**, 4923 (1976).
- [49] H. G. Bohn, W. Zinn, B. Dorner, and A. Kollmar, Physical Review B **22**, 5447 (1980).
- [50] H. G. Bohn, A. Kollmar, and W. Zinn, Physical Review B **30**, 6504 (1984).
- [51] M. W. Pieper, J. Kötzler, and K. Nehrke, Physical Review B **47**, 11962 (1993).
- [52] Y. Hasegawa and T. Nakanishi, in *Handbook on the Physics and Chemistry of Rare Earths*, Vol. 47 (Elsevier, 2015) pp. 101–146.